Synthesis and Photoluminescence of Three Bismuth(III)-Organic Compounds Bearing Heterocyclic N-Donor Ligands

Journal:	*Dalton Transactions*
Manuscript ID	DT-ART-07-2020-002360.R1
Article Type:	Paper
Date Submitted by the Author:	04-Aug-2020
Complete List of Authors:	Adcock, Alyssa; Georgetown University, Department of Chemistry Ayscue, Russell; Georgetown University, Department of Chemistry Breuer, Leticia; Georgetown University, Department of Chemistry Verwiel, Chloe; Georgetown University, Department of Chemistry Marwitz, Alexander; Georgetown University, Department of Chemistry Bertke, Jeffery; Georgetown University, Department of Chemistry Vallet, Valérie; Universite Lille 1, Laboratoire PhLAM Réal, Florent; University of Lille, ; Laboratoire de Physique des Lasers Atomes et Molécules, Knope, Karah; Georgetown University, Department of Chemistry

Synthesis and Photoluminescence of Three Bismuth(III)-Organic Compounds Bearing Heterocyclic N-Donor Ligands

Alyssa K. Adcock,[a,†] R. Lee Ayscue III,[a,†] Leticia M. Breuer,[a] Chloe P. Verwiel,[a] Alexander C. Marwitz,[a] Jeffery A. Bertke,[a] Valérie Vallet,[b] Florent Réal,[b] and Karah E. Knope[,a]*

[a]Department of Chemistry, Georgetown University, 37th and O Streets, NW, Washington, D.C. 20057, USA.

[b]Université Lille, CNRS, UMR 8523-PhLAM-Physique des Lasers, Atomes et Molécules, F-59000 Lille, France

KEYWORDS: Bismuth, luminescence, structure-property relationships, computational analysis

ABSTRACT

Three bismuth(III)-organic compounds, $[Bi_4Cl_8(PDC)_2(phen)_4]\cdot 2MeCN$ (**1**), $[BiCl_3(phen)_2]$ (**2**), and $[Bi_2Cl_6(terpy)_2]$ (**3**), were prepared from solvothermal reactions of bismuth chloride, 2,6-pyridinedicarboxylic acid (H_2PDC), and 1,10-phenanthroline (phen) or

2,2';6',2''-terpyridine (terpy). The structures were determined through single crystal X-ray diffraction and the compounds were further characterized via powder X-ray diffraction, Raman and infrared spectroscopy, and thermogravimetric analysis. The photoluminescent properties of the solid-state materials were assessed using steady state and time-dependent techniques to obtain excitation and emission profiles as well as lifetimes. The compounds exhibit visible emission ranging from the yellow-green to orange region upon UV excitation. Theoretical quantum mechanical calculations aimed at elucidating the observed emissive behavior show that the transitions can be assigned as predominantly ligand-to-ligand and ligand-to-metal charge transfer transitions. The solid-state structural chemistry, spectroscopic properties, and luminescent behavior of the bismuth compounds are presented herein.

INTRODUCTION

Bismuth and bismuth-based materials have been utilized as pharmaceuticals, photocatalysts, and other solid-state materials,[1-7] due to their attractive materials properties including nontoxicity, high thermodynamic stability, and low cost.[2-4, 8-11] However, as compared to transition metal- and lanthanide-organic complexes, relatively limited examinations of structure-property relationships in main group metal complexes and extended networks have been reported. Recently; though, bismuth-based compounds have attracted increasing attention due, in part, to their unique photoluminescent behaviour.[12-23] Trivalent bismuth has a [Xe]$4f^{14}5d^{10}6s^2$ electron configuration and possesses lone pair electrons ($6s^2$) with variable stereochemical activity. This results in a flexible coordination environment ranging from a hemidirected to holodirected coordination sphere, a range of coordination numbers, and thus, the potential for novel structure-types.[14, 21-27] Yet, such structural diversity combined with the limited solubility and hydrolytic propensity of many Bi salt starting materials, can provide significant challenges for controlled synthesis and structure prediction. As such, developing fundamental knowledge of the synthesis and structural chemistry of bismuth-organic-based phases is not only crucial for overcoming such challenges but also can provide key insight into the role that structural features have on materials properties such as luminescence.

Several luminescent bismuth-organic compounds have been reported to date; [12-13, 19, 22, 28-29] however, identification of the energy transfer pathways is often non-trivial; a number of charge transfer (CT) and/or ligand emission processes can play a role in the resulting luminescence. Bismuth-organic compounds have been reported to exhibit luminescence across a range of colors including "white" light emission.[14] The origins of these emissive transitions have been attributed to ligand-to-metal charge transfer (LMCT), metal-to-ligand charge transfer (MLCT), intraligand transitions ($n \leftarrow \pi^*$)/($\pi \leftarrow \pi^*$) that are noticeably shifted from the free ligand emission, and/or intraconfigurational $^1P_1 \rightarrow {}^1S_0$ and $^3P_1 \rightarrow {}^1S_0$ transitions originating from the $6s^2$ closed shell Bi^{3+} metal center.[14-19, 28, 30] Intervalence charge transfer has also been recently reported for several Bi systems.[22, 29] Additionally, the luminescent behavior of several halobismuthates have been attributed to a combination of metal-centered *sp* excited states and halogen-to-metal charge transfer (XMCT).[12, 31] Given the number of plausible energy transfer pathways that generally produce similar broad visible emission, a combined experimental and computational approach is essential for identifying structure-property relationships and elucidating the underlying luminescent mechanisms.

In this work, three compounds built from molecular Bi(III)-chloride complexes capped by N-donor ligands, 2,2',6,2"-terpyridine (terpy), 1,10-phenantroline (phen), and 2,6-pyridinedicarboxylic acid (PDC), were synthesized under solvothermal conditions. Selection of the ligands was based on several factors. Beyond their precedence in luminescent materials research, [32-35] these ligands have been shown to restrict dimensionality through capping coordination modes to yield molecular units. [36-40] Moreover, the aromaticity of the ligands may promote supramolecular interactions such as $\pi-\pi$ stacking, which have been shown to impact the materials properties of hybrid inorganic-organic complexes.[41] The obtained compounds, $[Bi_4Cl_8(PDC)_2(phen)_4]\cdot 2MeCN$ (**1**), $[BiCl_3(phen)_2]$ (**2**), and $[Bi_2Cl_6(terpy)_2]$ (**3**), were structurally characterized via X-ray diffraction studies and found to vary in nuclearity from mononuclear species (**2**) to dimeric units (**3**) to pseudo-tetrameric complexes (**1**). To the best of our knowledge, the pseudo-tetramers observed in **1**, which are bridged through carboxylate linkages and exhibit long Bi---Cl---Bi interactions between adjacent dimers, are unique within bismuth structural chemistry. Though the structure of compound **2** was previously described by White et al., the photoluminescence properties of this phase were not reported.[42] As such, **2** is included in this report to aid in the discussion of relevant structure-property relationships. The photoluminescent properties of **1-3** were explored through steady-state and time-dependent techniques. Each compound displayed visible light emission with room temperature lifetimes on the order of 10^{-6} s. Quantum mechanical calculations using structural models obtained from the experimentally determined single-crystal structures were performed to better understand the origins of the observed emissive pathways. The excitation and emission transitions for **1-3** are attributed to MLCT and LMCT pathways, respectively. Furthermore, corresponding electron density calculations suggest these CT pathways are facilitated between Bi-halide subunits and N-donor ligands. Through this investigation, valuable insight into structural features that potentially impart and/or influence luminescent properties is provided.

EXPERIMENTAL SECTION

Materials

Bismuth (III) chloride (Acros Organic, 98+%), 2,6-pyridinedicarboxylic acid (Alfa Aesar, 98%), 2,2';6',2''-terpyridine (Alfa Aesar, 97%), 1,10-phenanthroline (Acros Organics, 99+%), ethanol (Warner Graham Company), and acetonitrile (Fisher) were used as received. Nanopure water (≤0.05 μS; Millipore, USA) was used in all experiments.

Synthesis

$[Bi_4Cl_8(PDC)_2(phen)_4]$•2MeCN (1)

Bismuth chloride (0.0313 grams, 0.1 mmol), 2,6-pyridinedicarboxylic acid (0.0165 grams, 0.1 mmol), 1,10-phenanthroline (0.0180 grams, 0.1 mmol), and acetonitrile (3 mL) were loaded into a Teflon-lined stainless-steel autoclave. The autoclave was heated statically at 150° for 24 hours in an isothermal oven, then removed from the oven, and allowed to slow cool to room temperature over four hours. The reaction vessel was left undisturbed for one week after which the products were collected, washed with ethanol, and allowed to dry under ambient conditions. Colorless, thick needles of **1** were obtained along with a minor impurity identified as **2** via PXRD. Manual separation of **1** based on morphology allowed for yield estimation and subsequent bulk characterization. Note that crystals of both **1** and **2** were observed when the reaction vessel was opened immediately after cooling to room temperature; however, manual separation was not successful in these trials with shorter cooling times. Estimated yield of **1**: 40% (based on Bi). Elemental Analysis for $C_{66}H_{44}Bi_4Cl_8N_{12}O_8$: Calc. (Obs.): C, 35.18 (34.95); H, 1.98 (1.74); N, 7.46

(7.17%). Raman **1**: û = 1658, 1590, 1518, 1453, 1421, 1300, 1105, 1053, 1027, 724, 557, 518, 422, 286, 250 cm^{-1}.

[BiCl$_3$(phen)$_2$] (2)

Although **2** could be prepared solvothermally as a minor product as described above, in order to obtain sufficient product for bulk characterization the compound was prepared following a published synthesis.[42] Bismuth chloride (0.25 g, 0.79 mmol), 1,10-phenanthroline (0.43 grams, 2 mmol), and acetonitrile (20 mL) were heated under reflux with constant stirring (500 rpm). After two hours the white solid that was initially observed gradually turned faint pink; the pink solid was isolated via filtration. Further steps as described in the published synthesis to obtain single crystals including extraction into dimethyl sulfoxide/dichloromethane and evaporation were not performed, as single crystals sufficient for structure determination were obtained from the synthesis that yielded **1**. Yield: 87% (based on Bi). Elemental Analysis for $C_{24}H_{16}BiCl_3N_4$: Calc. (Obs.): C, 42.65 (42.77); H, 2.39 (2.26); N, 8.29 (8.28 %).

[$Bi_2Cl_6(terpy)_2$] (3)

Bismuth chloride (0.0319 g, 0.1 mmol), 2,6-pyridinedicarboxylic acid (0.0164 g, 0.1 mmol), 2,2’:6’,2’’-terpyridine (0.0236 g, 0.1 mmol), and acetonitrile (5 mL) were loaded into a 23 mL Teflon-lined stainless-steel autoclave. The autoclave was heated statically at 150° for five days in an isothermal oven, after which the autoclave was removed from the oven and allowed to cool to room temperature overnight. Large, rectangular prisms of **3** were collected, washed with ethanol, and allowed to dry under ambient conditions. Yield: 83% (based on Bi). Elemental Analysis for $C_{30}H_{22}Bi_2Cl_6N_6$: Calc. (Obs.): C, 32.83 (32.86); H, 2.02 (2.13); N, 7.66 (7.70%). Raman **3** $\hat{\upsilon}$ = 1591, 1563, 1497, 1482, 1456, 1331, 1302, 1288, 1116, 1080, 1042, 1005, 827, 721, 655, 403, 301, 271, 250 cm^{-1}.

Bulk Characterization Methods

Powder X-ray diffraction data were collected for bulk samples from which compounds **1**-**3** were isolated (Figs. S4-S8) using Cu-Kα radiation (λ = 1.542 Å) on a Rigaku UltimaIV with a rotation speed of 1 degrees/min from 3-40 degrees 2θ. Combustion elemental analysis was performed on a Perkin Elmer Model 2400 Elemental Analyzer for C, H, and N determination. Thermogravimetric analyses were conducted for **1** and **3** on a TA Instruments Q50 Thermogravimetric Analyzer under flowing air (60 mL/min) from 50 to 600 °C with a step speed of 5 °C/min (Figs. S18-S19). UV-vis absorption spectra for solid samples of **1-3** were collected on an Agilent Technologies Cary 5000 UV/Vis-NIR instrument using a diffuse reflectance attachment. Spectra (Figs. S15-S17) were collected over 200-800 nm using the Cary WinUV program. Raman spectra were collected on single crystals pulled from the bulk sample using an excitation source of 532 nm (maximum power=100mW) on a Horiba LabRAM HR Evolution Raman Spectrometer. Spectra of **1** and **3** (Figs. S22-S23) were recorded from 200 to 2200 cm^{-1} using 20 accumulations and a laser power between 3.2 to 10%.

Structure Determination via Single Crystal X-ray Diffraction

Single crystals of **1-3** were isolated from the bulk samples and mounted in N-paratone on MiTeGen micromounts. Single crystal X-ray diffraction data were collected at 100(2) K on a Bruker D8 Quest diffractometer equipped with an I*μ*S X-ray source (Mo-Kα radiation;

λ=0.71073 Å) and a Photon 100 detector. Each data set was integrated using the SAINT software package included with APEX3.[43-44] An absorption correction was applied using a multi-scan technique in SADABS.[44] The structures were then solved using direct methods via SHELXT and refined by full-matrix least-squares on F2 using the SHELXL software in SHELXLE.[45-46] Crystallographic data are provided in Table 1, and full refinement details as well as CIF data are available as Supporting Information. CIF data for **1**-**3** were also submitted to the Cambridge Crystallographic Data Centre (CCDC), www.ccdc.cam.ac.uk/by, and may be obtained by referencing numbers 1841302-1841304. While the structure of **2** at 295 K was previously reported, [42] a low temperature dataset for **2** was collected at 100 K for the sake of comparison with the structures reported herein. Intermolecular interactions for all compounds were assessed using the PLATON software suite.[47]

Luminescence Measurements

Excitation and emission spectra were collected on a Horiba PTI QM-400 Spectrofluorometer at room temperature on ground solid samples (Figs. S9-S11). Long pass filters were used to remove harmonic signatures. Time-resolved measurements to determine lifetime values were acquired at room temperature using a Xenon flash lamp as the average of 10,000 shots. Decay curves were plotted and fit using Origin Pro 8.5 (Figs. S12-S14). Lifetime values given are the average of three independent determinations taken at the maximum excitation and emission wavelengths.

Computational Studies

Structural models obtained from the single crystal structures were used to calculate the absorption spectra in an effort to identity the transitions involved in the observed photoluminescence spectra. Clusters of various sizes were rendered and used for analysis, starting from a single molecular unit to larger systems (dimer, trimer, and pseudo-tetramer). All spectra were computed using a similar approach proposed by Sorg et al., [17] based on single point calculations using a current development version of the ORCA 4.3 program package.[48-49] The calculations rely on the use of the CAM-B3LYP functional, a hybrid functional with long-range separation, to compute the density of the compound, [50] associated to def2-SVP basis set for all atoms, [51] and a Relativistic Small

Core Effective Pseudopotential for Bi. [52] To accelerate the calculations, two approximations were used: the RI and chain-of-spheres (COSX) approximations (grid X5). [53-54] The absorption energies and oscillator strengths were computed by means of the sTDA (simplified Tamm-Dancoff approach) method, [55-57] which allows a reasonable qualitative description of large-system spectra. Spin-orbit coupling has been neglected as no change in the spectral envelopes was observed for the monomer $BiCl_3(phen)_2$ in compound **1** (See Discussion in Section VII of the SI). An energy cut-off at 5 eV was used, and spectra were normalized over a region between 250 up to 450 nm. For the non-zero absorption states, a Lorentzian function was added on top of each pick, with various widths in order to account for the natural broadening observed at ambient temperature.

Additional analysis was performed using the ADF package. [58-60] Analysis of the bonds between the metal and the ligands were realized using the ETS-NOCV (Extended Transition State Natural Orbitals for Chemical Valence) analysis method available in the ADF package, with the PBE0 functional. The molecular complex was partitioned into two fragments, the first one being the $BiCl_3$ subunit and the second the phen groups. [61-62]

RESULTS AND DISCUSSION

Synthetic Considerations

Synthetic avenues to access bismuth-based materials can be challenging, in part, due to the limited solubility of bismuth precursors and the hydrolytic instability of bismuth. The reaction for **1** also produced **2** as a minor impurity; therefore, manual separation of the phases was necessary to perform subsequent characterization and achieve phase purity of **1**. Extensive variation of reaction parameters was performed in an attempt to afford a phase-pure product of **1** but proved unsuccessful. Although it was not incorporated into the solid-state structure of **3**, 2,6-H_2PDC was added to the reaction and seemingly enabled improved crystallization of **3** to yield large block crystals. Absent this organic “spectator”, a microcrystalline powder of **3**, along with a BiOCl impurity that originates from partial hydrolysis of $BiCl_3$, was obtained (Fig. S8). Solvothermal reactions were used to help mitigate formation of bismuth oxychloride. Furthermore, the addition of H_2PDC may help drive formation of **3** and subsequently preclude formation of BiOCl; although, the exact role of H_2PDC is unknown. Reactions with other organic species (2,5-H_2PDC and 3,4-H_2PDC) were performed in attempt to obtain other novel phases; however, **3** was the only phase observed.

Structure descriptions

The single crystal structures of **1-3** were determined at 100 K using single crystal X-ray diffraction. The structure of **2** at 295 K has been previously reported; however, for the sake of comparison with **1** and **3**, a low temperature dataset was collected at 100 K. The structure of each compound consists of discrete molecular units, varying in nuclearity from mononuclear moieties in **2** to dimeric units in **3** to pseudo-tetrameric species in **1**.

Table 1. Crystallographic structure refinement details for **1**- **3**.

	1	**2**	**3**
Chemical formula	$C_{66}H_{44}Bi_4Cl_8N_{12}O_8$	$C_{24}H_{16}BiCl_3N_4$	$C_{30}H_{22}Bi_2Cl_6N_6$
MW ($gmol^{-1}$)	2252.67	675.75	1097.21
T (K)	100(2)	100(2)	100(2)
λ (Mo Kα)	0.71073	0.71073	0.71073
μ (mm^{-1})	10.813	8.433	11.446
Crystal system	Triclinic	Monoclinic	Monoclinic
Space group	*P-1*	$P2_1/c$	$P2_1/n$
a (Å)	9.7898(6)	9.6115(3)	12.7368(6)
b (Å)	13.7846(13)	31.7985(1)	9.4838(4)

c (Å)	27.4465(18)	7.5977(2)	13.6313(6)
α (°)	102.725(2)	90	90
β (°)	90.442(2)	109.328(1)	102.0880(10)
γ (°)	110.737(2)	90	90
Volume (Å^3)	3363.9(4)	2191.22(11)	1610.06(12)
Z	2	4	4
R_{int}	NA[a]	0.0224	0.0567
R (I > 2σ)	0.0270	0.0152	0.0247
wR_2	0.0627	0.0317	0.0635
GooF	1.076	1.166	1.099
CCDC number	1841302	1841303	1841304

[a] The refinement of 1 was processed as a two component twin and therefore, an R_{int} is not reported. Moreover, compound 2 (295 K) was previously reported and can be found by referencing PURQUO. [42]

$[Bi_4Cl_8(PDC)_2(phen)_4]$•2MeCN (1)

The solid-state structure of **1** is built from four crystallographically unique bismuth(III) ions, eight chloride ions, four bidentate phen ligands, and two PDC ligands. Bi1 and Bi3 are both seven coordinate, bound to three chloride ions, two nitrogen atoms from one κ^2-phen, and two oxygen atoms from PDC. The Bi1-O distances are 2.5498(2) and 2.7644(2) Å, the Bi1-Cl distances range from 2.6678(2) to 2.7021(2) Å, and the Bi1-N distances are 2.4538(2) and 2.4806(2) Å. In the case of Bi3; however, the Bi3-O distances are 2.5854(2) and 2.7926(2) Å, the Bi3-Cl distances range from 2.6333(2) to 2.6864(2) Å, and the Bi3-

N distances are 2.4424(2) and 2.5008(2) Å. Bi2 and Bi4 are both six coordinate, bound to one chloride ion, three nitrogen atoms from one κ^2-phen and one PDC, and two oxygen atoms from the PDC. The Bi2-O distances are 2.5609(2) and 2.2869(1) Å and the Bi2-N distances range from 2.4406(2) to 2.5875(2) Å. The Bi2-Cl4 distance is 2.4917(2) Å, and two long Bi---Cl interactions are observed as 3.2081(2) and 3.4579(2) Å.[63] The Bi4-O distances are 2.5633(2) and 2.2811(1) Å, with the Bi4-N distances ranging from 2.4271(2) to 2.5745(2) Å. The Bi4-Cl8 distance is 2.4917(2) Å, and two long Bi---Cl interactions are observed as 3.2147(2) and 3.4905(2) Å. Bi1 and Bi2 are bridged through one oxygen atom (O52) of the carboxylate of the PDC ligand, forming dimeric units. These dimers interact through two chloride atoms (Cl2 and Cl3) to form pseudo-tetramers as depicted in Fig. 1. Bi3 and Bi4 are similarly bridged through the carboxylate of one PDC ligand (O62) to form dimeric units that are then further bridged into pseudo-tetramers through relatively long Bi---Cl---Bi interactions involving two chloride atoms (Cl6 and Cl7). While one outer coordination sphere acetonitrile molecule per formula unit was resolved during the refinement, residual electron density existed outside the cluster. This residual electron density may be attributed to an additional ACN molecule; however, disorder precluded modeling of these atoms, and the model was squeezed to remove the residual electron density. Several intermolecular π-π interactions are observed between the phen and pyridine rings of the pseudo-tetramers, further stabilizing the crystal structure. As shown in Fig. 2a, moderate π-π stacking interactions exist between the phen ligands bound to Bi1 and Bi3 (designated as phen1 and phen3, respectively). These interactions were tabulated in Platon[47] and the strongest interactions exhibit $C_{phen3}\cdots C_{phen1}$ distances of 3.5088(2) Å with a slip angle equal to 18.4°. Weaker interactions exist between the pyridine rings of each PDC ligand and the phen ligands bound to Bi2 or Bi4, as depicted in Fig. 2b. For the PDC bound to Bi1 and Bi2 (PDC5) and the phen bound to Bi2 (phen2), $C_{phen2}\cdots C_{PDC5}$ distances are 3.8167(3) Å with a slip angle of 20.2°. In the case of the PDC bound to Bi3 and Bi4 (PDC6) and the phen bound to Bi4 (phen4), the $C_{phen4}\cdots C_{PDC6}$ distance is 3.8811(3) Å with a slip angle of 24.6°.

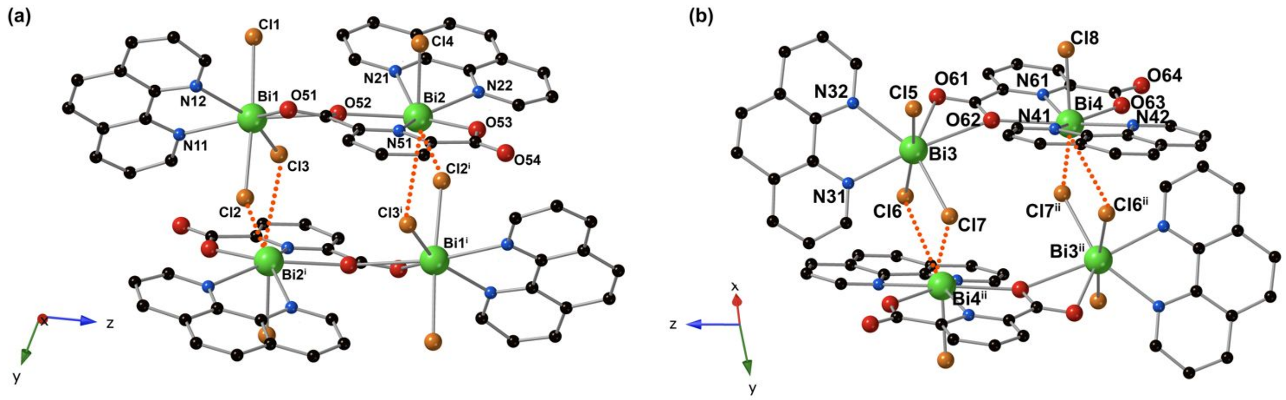

Fig. 1. Illustration of the two unique tetrameric units in **1** which are built from (a) Bi1 and Bi2 and (b) Bi3 and Bi4. Green, red, orange, blue, and black spheres represent bismuth, oxygen, chlorine, nitrogen, and carbon atoms, respectively. Dotted orange lines denote long Bi---Cl interactions. Hydrogen atoms and acetonitrile solvent molecules have been omitted for clarity. Symmetry operators: (i) 2 - x, 1 - y, 1 - z; (ii) 1 - x, 1 - y, -z.

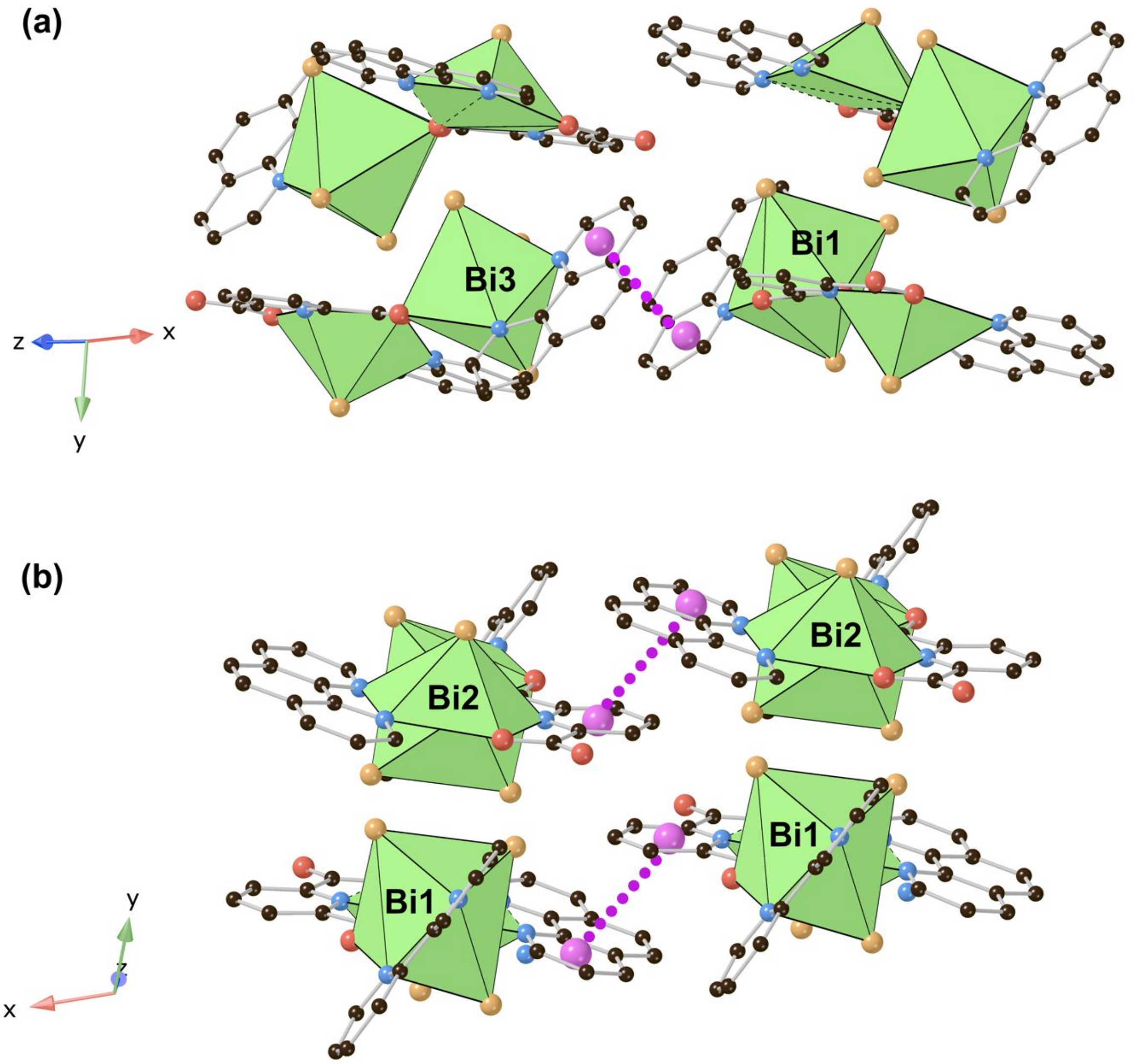

Fig. 2 Polyhedral representation of **1** showing π-π stacking interactions (purple dashed lines) between (a) two phenanthroline from adjacent Bi1, Bi2 and Bi3, Bi4 tetramers and (b) phen and PDC from two Bi1, Bi2 tetramers. Green polyhedra, red, orange, blue, and black spheres represent bismuth, oxygen, chlorine, nitrogen, and carbon atoms, respectively. Purple spheres represent ring centroids. Hydrogen atoms and acetonitrile solvent molecules have been omitted for clarity.

$[BiCl_3(phen)_2]$ (2)

As the structure of **2** has been previously reported, only a brief structural description is provided here. Compound **2** is built from one crystallographically unique bismuth(III) metal center, three chloride ions, and two bidentate phen ligands. The bismuth ion is seven coordinate, bound to three chloride ions and four nitrogen atoms from the phen ligands (Fig. 3). The Bi-Cl bond distances range from 2.598(1) to 2.748(1) Å, and the Bi-N distances range from 2.476(2) to 2.771(2) Å. Intermolecular π-π stacking interactions are observed throughout the structure between adjacent phen rings, with the distance between the centroids $C_{phen}\cdots C_{phen}$ found to be 3.7557(1) Å with a slip angle of 22.2°.

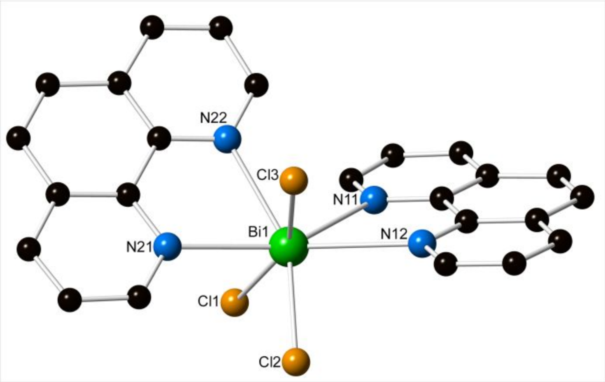

Fig. 3 Illustration of the monomeric unit in **2**. Green, orange, blue, and black spheres represent bismuth, chlorine, nitrogen, and carbon atoms, respectively. Hydrogen atoms have been omitted for clarity.

$[Bi_2Cl_6(terpy)_2]$ (3)

The structure of **3** is built from one crystallographically unique trivalent bismuth ion, one tridentate terpy, and three chloride ions. Each metal center is seven coordinate, adopting a distorted pentagonal bipyramidal coordination geometry, bound to three nitrogen atoms from the terpy ligand and four chloride atoms. The Bi-Cl distances range from 2.592(1) to 2.814(1) Å, while the Bi-N bond distances range from 2.479(3) to 2.626(3) Å. As seen in Fig. 4, bridging chloride atoms, Cl1 and Cl1', link the bismuth metal centers to form discrete molecular dimers. No significant π-π stacking interactions are present between the terpy rings.

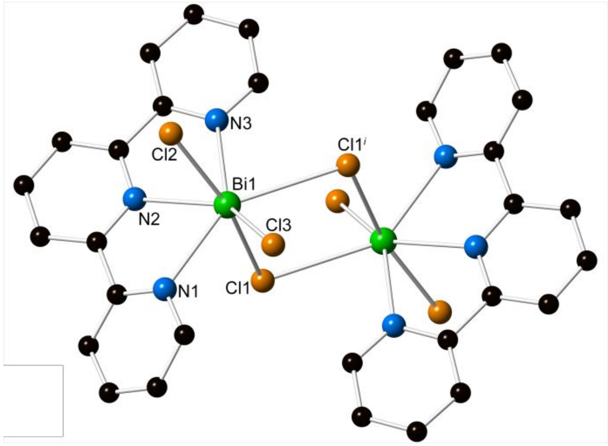

Fig. 4 Illustration of the dimeric units in **3**. Green, orange, blue, and black spheres represent bismuth, chlorine, nitrogen, and carbon atoms, respectively. Hydrogen atoms have been omitted for clarity. Symmetry operators: (i) -x, -y + 1, -z + 1.

Structural analysis

More than eighty bismuth-organic compounds containing either bound phen or 2,6-H_2PDC have been reported; the majority exist as either discrete monomeric or dimeric units or crystallize as extended networks. Zhang and Feng, for example, synthesized a dimeric bismuth compound containing both 2,6-H_2PDC and phen, $[Bi_2(2,6\text{-}PDC)_2(N_3)_2(phen)_2]\cdot 4H_2O$ under ionothermal conditions wherein the bismuth metal centers are bridged through the carboxylate oxygen atoms of the PDC.[64] To the best of our knowledge, **1** marks the first reported bismuth pseudo-tetramer decorated with phen and/or 2,6-PDC ligands. In the Cambridge Structural Database 2020, reports of discrete chlorobismuth tetramers are limited. Approximately eight chlorobismuth tetramers with organic ligands bound directly to the bismuth metal center have been described. Most of the tetramers reported are polychlorobismuthates, with the general formula $[Bi_4Cl_x]^{12-x}$ (where x=16, 18, or 20), that are charge balanced by outer coordination sphere metal and/or ligand cations. Dimeric motifs such as that observed in **3** are common structural units in bismuth-organic materials literature; however, **3** is the first example of a bismuth-terpy species with chloride in the inner coordination sphere of the metal. Five of the reported bismuth-terpy species contain either bound nitrate or iodine originating from the respective bismuth salt used in the reactions.[65-68] We have also previously reported a mixed ligand Bi-terpy-thiophenemonocarboxylate compound.[37] The structural unit of **3** is isostructural to the bromobismuth-phen dimer published by White et al., $[Bi_2Br_6(phen)_4]$, though attempts by the authors to produce the chloride analog were reportedly unsuccessful.[42] Interestingly, the chlorobismuth dimer is accessible using terpy as a capping ligand, possibly owing to the increased denticity and ability of terpy to better saturate the metal coordination sphere. Furthermore, it is of note that while the structure of **1** exhibits a coordination environment consistent with the presence of a stereochemically active lone pair, as evidenced by the distorted metal coordination geometry, apparent open face, and elongation of Bi---Cl interactions, [23, 26, 69] little evidence of lone pair activity about the Bi centers is present in **2** and **3**.

Photoluminescence

Luminescence spectra for each compound were collected on bulk solid samples at room temperature. The luminescence spectra of the free ligands H_2PDC, phen, and terpy were collected and are reported in the ESI (Figs. S9-S11). Upon excitation of the free ligands at 343, 363, and 348 nm, respectively, broad emission bands centered between 370-430 nm were observed. Compounds **1-3** exhibit broad visible light emission peaks centered at 570, 590, and 537 nm, respectively, as shown in Figs. 5-6. A summary of excitation and emission maxima along with lifetime measurements for the reported compounds is provided in Table 2. Room temperature time-resolved luminescence studies revealed that **1** displayed short-lived luminescence lifetimes with a biexponential decay of 8(1) μs and 76(3) μs (Fig. S12). Longer biexponential decays of 14(1) μs and 241(4) for **2** and 10(1) and 196(4) for **3** were observed (Figs. S13-14).

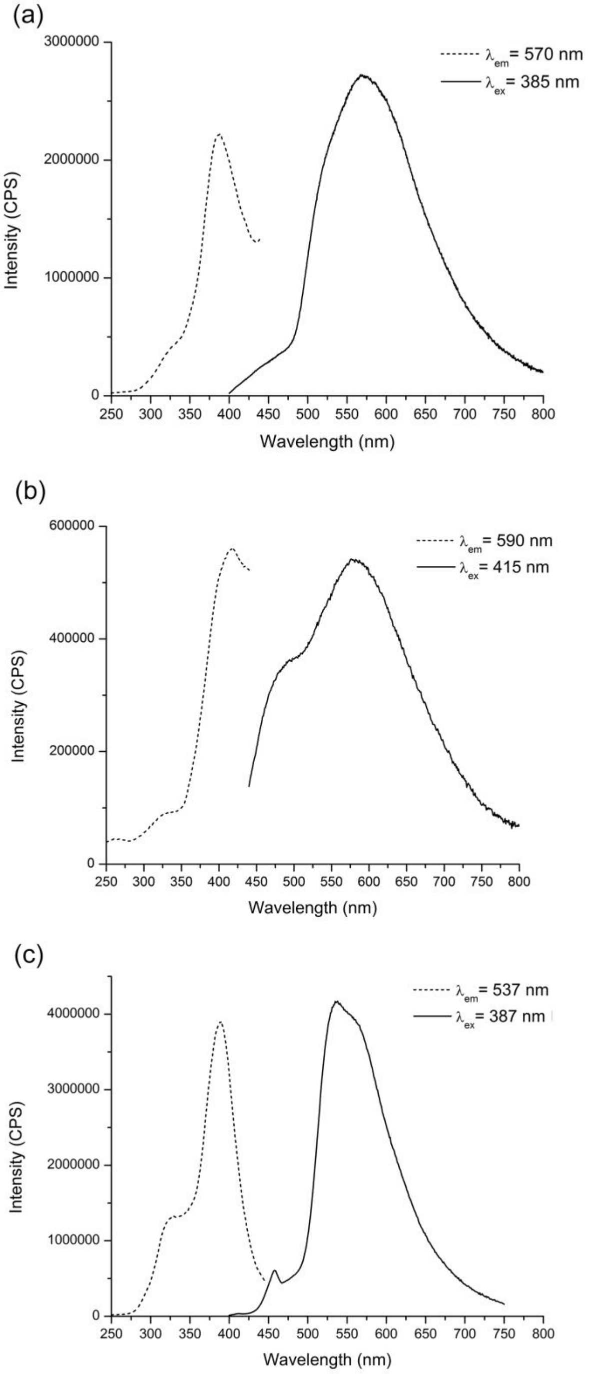

Fig. 5 Room temperature excitation (dashed) and emission (solid) spectra for (a) **1**, (b) **2**, and (c) **3**.

Table 2. Photophysical measurements for **1-3**.

	Maximum excitation (nm)	Maximum emission (nm)	Lifetime (μs)
1	385	570	8(1), 76(3)
2	415	590	14(1), 241(4)
3	387	537	10(1), 196(4)

For each compound, the Commission Internationale L'Eclairage (CIE) coordinates were determined from the emission profile and are plotted in Fig. 6. Each compound displays visible yellow-green to orange emission upon exposure to UV light as confirmed by the solid-state luminescence measurements.

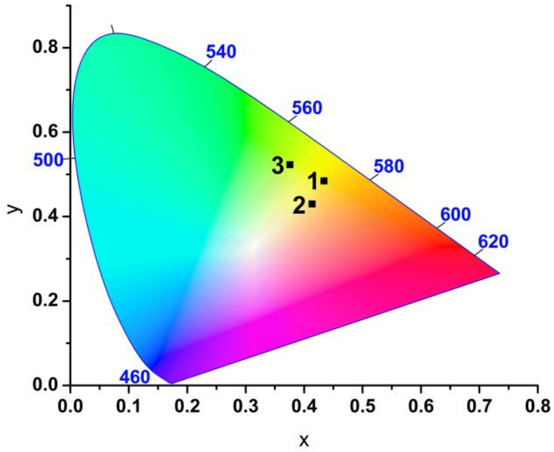

Fig. 6 Room temperature CIE chromaticity coordinates for **1**-**3**.

To further our insight into the electronic states and possible transitions correlating to the reported luminescence, quantum mechanical methods have been applied using the ORCA

4.3 software package.[48] Various cluster cut-outs of each compound were rendered and used as model systems to compute theoretical UV-Vis absorption spectra. These theoretical spectra were compared to the experimentally obtained optical absorption spectra (Figs. S15-S17). Additionally, molecular orbitals (MOs) involved in the main excitation bands of the absorption spectra were calculated for each compound. While there is a degree of uncertainty in the calculated transition wavelengths and oscillator strengths, the combined theoretical and experimental data have provided insight into the transitions responsible for the emissive behavior of the compounds.

For **1**, several cluster cut-outs were prepared and used for subsequent calculations, including the as-reported pseudo-tetramer, $[Bi_4Cl_8(PDC)_2(phen)_4]$, and several dimers of tetramers, $[Bi_4Cl_8(PDC)_2(phen)_4]_2$. Looking at the general shape of the spectra (Fig. 7), the different renderings of the pseudo-tetramers do not exhibit fundamental differences. Table 3 lists the position of the lowest states for each "dimer" of tetramers, showing that the lowest part could be split into two regions separated by a frontier at 390 nm. For simplicity, our analysis focused on the strong absorption peaks located at 350 nm and ~400 nm of one of the tetramer cut-outs (C). Decomposition of the peaks is reported in Table 4 and the MOs involved in the absorption process are depicted in Fig. 8.

The lower energy bands involve excitation from the bismuth-chloride subunit to the phen groups (HOMO-1 → LUMO+2) in a "metal"-to-ligand charge transfer (Fig. 8). Different than typical MLCT, there is strong mixing between the chloride orbitals and that of the Bi^{3+} ion; thus, the likely excited state involved in the CT process does not exclusively have metal character but involves the whole $BiCl_3$ subunit. Upon de-excitation, these transitions should correspond to a ligand-to-metal subunit charge transfer (LMCT).

Interestingly, the calculations show that the PDC ligand does not appear to be involved in CT at lower energies. However, higher energy absorption bands can be attributed to ligand-to-ligand charge transfer between the ligands, resulting in underlying ligand emissions which are supported by experimentally observed biexponential decay. To further explore the absorption, the calculated spectra (solid lines) were compared to the experimental absorption spectrum (black dashed line) (Fig. 7b). The intensity of the simulated spectrum was scaled for easier comparison. From the overlay, the general shape of the theoretical spectrum is in reasonable agreement with the experimental data. Moreover, in the lower part of the spectra, the more intense singlet to singlet excitations are about 395 nm, a value that matches the 385 nm excitation wavelength used for the experimental characterization of the compound.

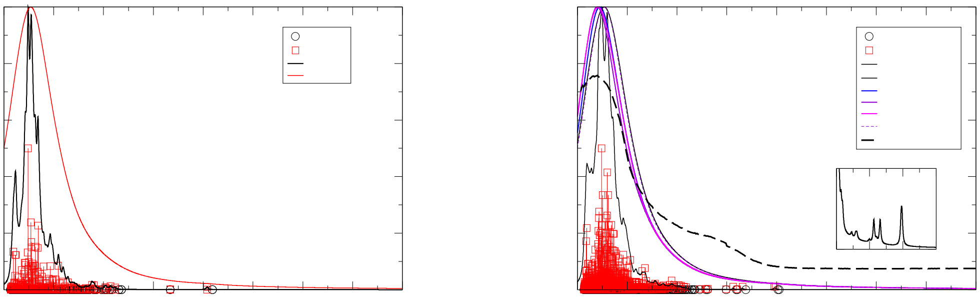

(a) **1** monomer (b) **1** dimer

Fig. 7 (a) Computed UV-vis absorption spectrum of **1** with two different Gaussian heights (black and red solid lines) calculated with one tetramer. (b) Computed UV-vis absorption spectrum of **1** calculated with two tetramers in various orientations (C, D, E, & F) overlaid with the experimental absorption spectrum (black dashed line). The lower part of the theoretical spectrum is reported in the box (squares represent the position of all the states in that specific region).

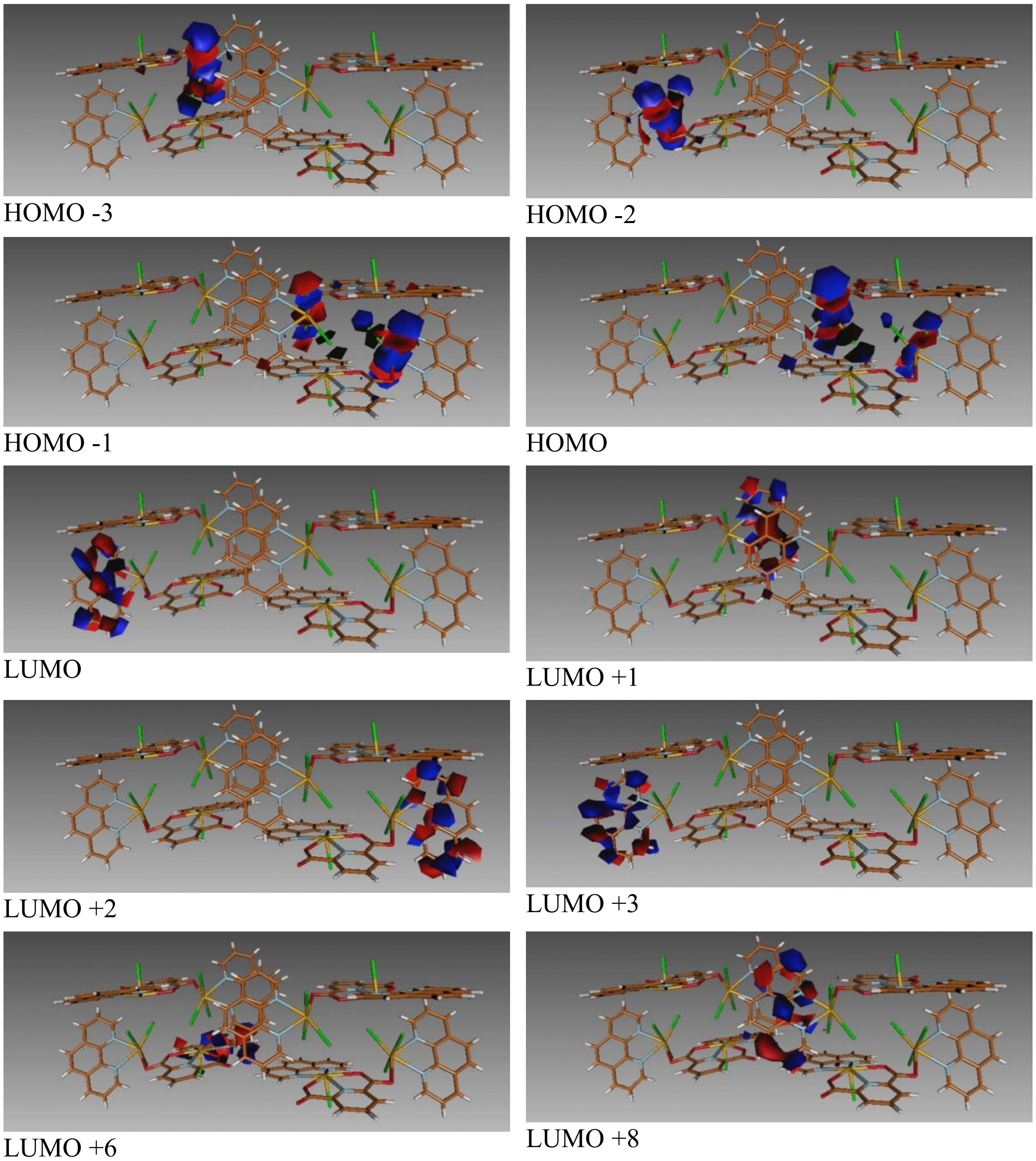

HOMO -3

HOMO -2

HOMO -1

HOMO

LUMO

LUMO +1

LUMO +2

LUMO +3

LUMO +6

LUMO +8

Fig. 8 Molecular orbitals implied in the main low-lying excitations of **1**. Note that the cut-out shown is for a "dimer" of tetramers.

Table 3. Lowest absorption wavelengths of singlet states (nm) of various renderings (C, D, E, F) of "dimers" of tetramers for **1.**

λ_C (nm)	λ_D (nm)	λ_E (nm)	λ_F (nm)
398.4	406.2	403.2	398.4
397.2	406.2	403.2	398.3
-	393.6	401.2	386.4
-	393.5	401.2	386.4
366.2	-	-	-

360.7	-	-	-
356.6	368.2	365.5	350.6
349.6	368.2	365.5	350.6
330.4	357.4	363.3	341.1
329.1	357.4	363.3	341.1
322.9	314.3	309.2	308.5

Table 4. Decomposition of the main singlet to singlet excitations of **1**.

λ (nm)	Decomposition of the main singlet to singlet excitations
398.4	-0.99 (HOMO-1→ LUMO+2)
397.2	-0.77 (HOMO-1→ LUMO+2) -0.63 (HOMO→ LUMO+1)
366.2	0.98 (HOMO-3→ LUMO+1) -0.11 (HOMO-2→ LUMO+8)
360.7	-0.99 (HOMO-2→ LUMO+6)
356.6	0.60 (HOMO→ LUMO+8) -0.48 (HOMO-1→ LUMO+8) 0.40 (HOMO→ LUMO+3)
349.6	-0.76 (HOMO→ LUMO+6) -0.63 (HOMO→ LUMO+8)

For the neutral monomer in **2**, three cluster sizes were prepared including the as-reported monomer, [$BiCl_3phen_2$], a pseudo-trimer built from three monomeric units, [$BiCl_3phen_2$]$_3$, and a pseudo-tetramer built from four monomeric units, [$BiCl_3phen_2$]$_4$. When looking at the electron distribution of the electronic ground state, it is worth noting that the $BiCl_3$ subunit tends to strongly attract the electrons from the two donor groups, though predominately from the one with the shortest Bi-N distances. The Mulliken population analysis yields a total charge on the bismuth center of 1.5 e^-, indicating some degree of covalency between bismuth and the phen groups. The deformation density shown in Fig. 9 nicely supports the fact that there is an accumulation of density on the $BiCl_3$ subunit (blue regions), along with a depletion in the N-donor ligands.

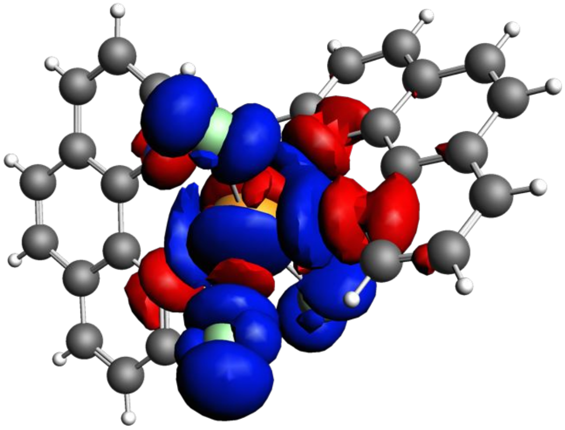

Fig. 9 Deformation density of **2**. The red areas correspond to a depletion of the density as compared to the isolated fragments ($BiCl_3$ and the two phenanthroline ligands), while the blue regions correspond to accumulation of electron density.

An important aspect that can be examined using quantum mechanical calculations is the qualitative evolution of the absorption spectra as a function of aggregate size. The absorption spectra at the SF level (Fig. 10) describe the effect of the Lorentzian width used to convolute the spectrum. The cluster aggregate size effects are illustrated in Fig. 10b. As shown in Fig. 10b, the main absorption bands above 350 nm are slightly affected by the size of the aggregate, going from the monomer (Fig. 10a) to the trimer (Fig. 10b), and the relative intensities of the two main bands evolve with respect to the size of the system. For example, the band at ~450 nm for the monomer is blue-shifted to 425 nm for the larger, linear trimer (Fig. 10b). The larger compound (tetramer) made of four subunits has a very similar spectrum (Fig. 10c) to that of the trimer (Fig. 10b).

The decomposition of the low-lying states is proposed in Table S1 and the MOs are represented in Figs. S25-S26 for the trimeric and tetrameric units, respectively. In the larger aggregates, the lowest energy bands (i.e. above 400 nm) correspond to excitation out of $BiCl_3$ centered orbitals to the π^* orbitals of the closest phen group (HOMO-2 → LUMO in the linear trimer; HOMO-1→ LUMO+5, LUMO+6, and LUMO+7 in the tetramer). The other bands (below 400 nm) are a combination of MLCT as expected for such types of compounds, and are in agreement with the recent work by Sorg et al [17] or Ouerghji et al. [70] Interestingly, the experimentally determined excitation wavelength used to collect the emission spectra is 415 nm, which agrees well with the lowest absorption energy predicted with the highest intensity in the low part of the spectrum (Fig. 10b) for a singlet to singlet excitation.

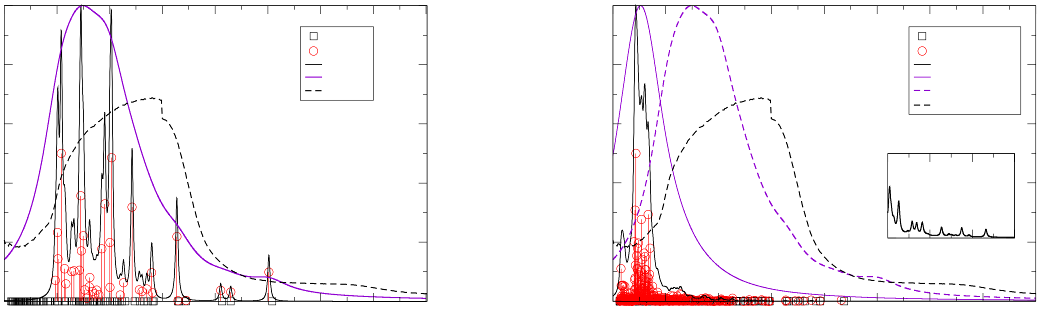

(a) **2** monomer (b) **2** trimer

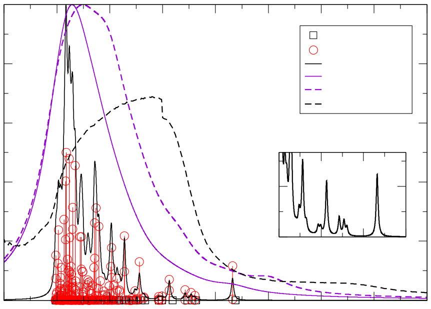

(c) **2** tetramer

Fig. 10 (a) Computed UV-vis absorption spectrum of **2** with two different Lorentzian widths (black and purple solid lines) calculated for one monomer. (b) and (c) Computed UV-vis absorption spectrum of **2** calculated with one monomer (dashed purple line) and trimer and tetramer (solid lines) of the monomer, respectively, overlaid with the experimental absorption spectrum (black dashed line). The lower part of the theoretical spectrum is reported in the inset (squares represent the position of all the states in that specific region).

For **3,** four cluster cut-outs were rendered: (i) the dimeric unit, [Bi_2Cl_6(terpy)$_2$], two different dimer of dimers (ii) [Bi_2Cl_6(terpy)$_2$]$_2$ with the ligands perpendicular to each other (ortho) and (iii) [Bi_2Cl_6(terpy)$_2$]$_2$ with the dimers in parallel to each other (in plane), and (iv) a tetramer of dimers, [Bi_2Cl_6(terpy)$_2$]$_{4.}$ As shown in Fig. 11, many bands are common between the considered systems. The region over 350-450 nm exhibits a dense absorption band. When going from the discrete dimer to larger cut-outs, an increase in the number of states is observed which is expected from larger aggregates. However, the main features of the spectra do not change substantially. In the lower energy part of the spectrum of the tetrameric unit, for example, there are three bands with relatively strong oscillator strength above 380 nm (see Table S2; MOs are shown in Fig. 12). The peak at 411 nm can be attributed to the excitation of the $BiCl_3$ subunit to nonbonding orbitals of the closest terpy groups belonging to the same molecular subsystem (HOMO-6 → LUMO+6, See Fig. 12). The two other lower wavelength absorption bands are more delocalized as the main contribution to the transition corresponds to an excitation of an electron localized on the $BiCl_3$ center to an orbital of the "opposite" terpyridine ligand (HOMO-15 → LUMO+1 and HOMO-14 → LUMO+2; Fig. 12). Based on the theoretical spectrum one would expect that three bands centered at 387, 395, and 411 nm may be used to probe the luminescence of the compounds; the optimal excitation wavelength determined experimentally was 387 nm.

Yet, agreement between the experimental absorption data and the simulation is rather poor, as shown in Fig. 11c. Two clear absorption bands are observed experimentally, located at 240 and 370 nm, with none above 400 nm, while the simulated data propose one main band at 240 and 275 nm and a second dense, but less intense region up to 430 nm.

Regarding the two previous cases and the existing coherence, no reasonable explanation for such a disagreement has yet been identified.

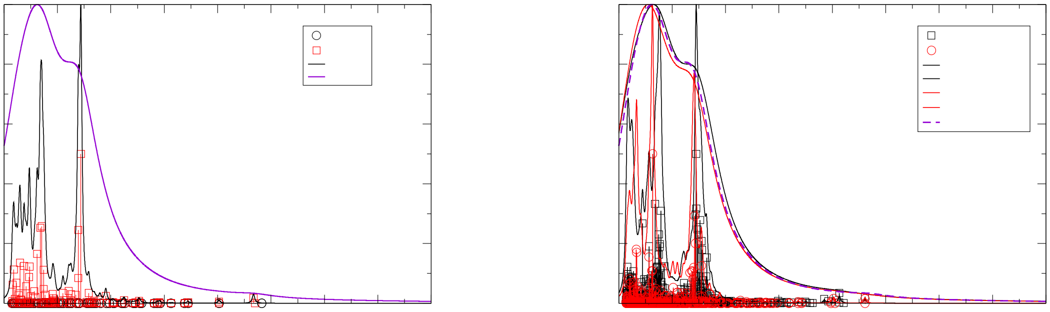

(a) **3** monomer (b) **3** dimer

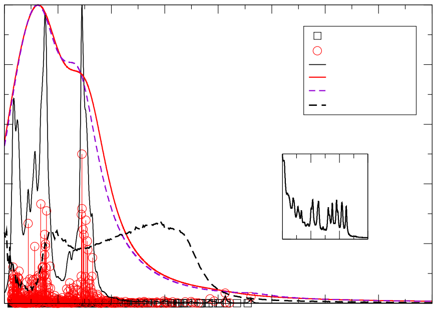

(c) **3** tetramer

Fig. 11 (a) Computed UV-vis absorption spectrum of **3** with two different Lorentzian (black purple solid lines) calculated with one monomer of dimer. (b) Computed UV-vis absorption spectrum of **3** calculated with one dimer (dashed purple line) and two dimers of dimer (solid lines) in two different orientations. (c) Computed UV-vis absorption spectrum of **3** calculated with one dimer (dashed purple line) and a tetramer of dimers (solid red line) overlaid with the experimental absorption spectrum (black dashed line). The lower part of the theoretical spectrum is reported in the box (squares represent the position of all the states in that specific region).

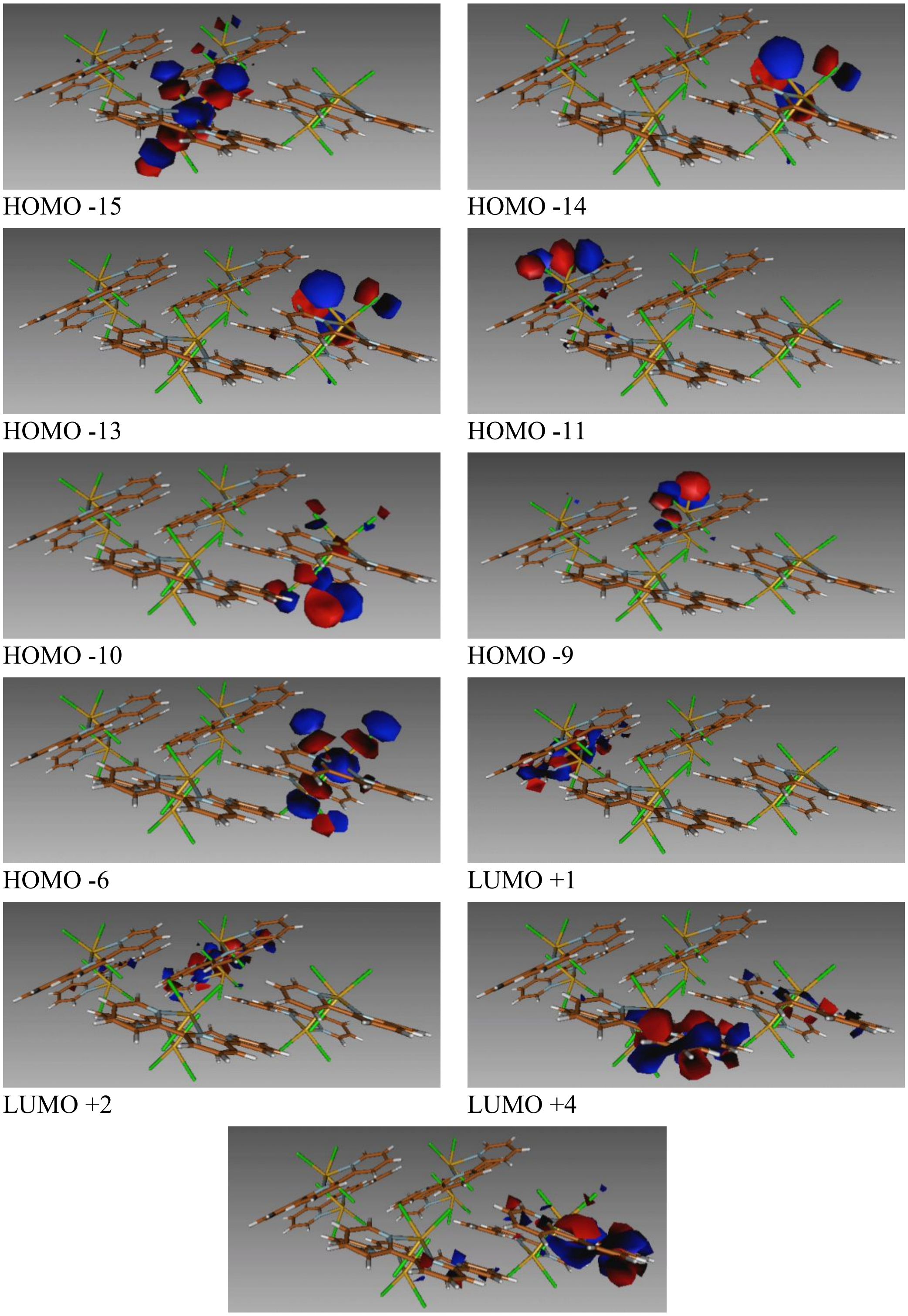

HOMO -15

HOMO -14

HOMO -13

HOMO -11

HOMO -10

HOMO -9

HOMO -6

LUMO +1

LUMO +2

LUMO +4

LUMO +6

Fig. 12. Molecular orbitals implied in the main first excitations of **3** for the tetrameric unit.

Our theoretical analysis compares well with other polychlorobismuth-organic compounds such as those reported by Müller-Buschbaum et al. concerning the luminescence of several chlorobismuth-4,4'-bipyridine coordination polymers.[17] Computational studies identified MLCT, originating from the occupied orbitals of the bismuth chloride subunit (in their case, Bi_2Cl_6) to ligand orbitals delocalized over several ligands, as being responsible for the excitation bands and subsequent emission resulting from the corresponding LMCT.

Thermal stability

The thermal stabilities of compounds **1** and **3** were investigated using thermogravimetric analysis under flowing air (Figs. S18-S19). For **1**, the total weight loss was 56.1% and occurred over four consecutive steps. The first weight loss of roughly 13 % occurred over 200-275 °C and is consistent with the loss of two MeCN and one phen. The second weight loss of 25.9% was complete by 350 °C, and the third weight loss (4.8%) was complete by 425 °C. Attribution of these steps is somewhat ambiguous, but the combined weight losses are consistent with decomposition of two phen groups and two PDC units. The final weight loss of 12.1% was complete by 600 °C and is consistent with the loss of one phen unit and three chloride ions (or alternatively seven Cl). For **3**, the total weight loss was 67.3% and occurred over two consecutive steps. The first weight loss of 23.5% occurred over 180 °C to ~300 °C, and the second weight loss of 43.8% was complete by 360 °C. Assignment of these steps remains unclear; however, in an effort to identify the thermal decomposition products, powder X-ray diffraction data was collected on the resulting powders. The PXRD pattern of the thermal decomposition product of **1** did not index to any known bismuth oxide, bismuth chloride, or bismuth oxychloride phase (Fig. S20). However, the PXRD pattern of the thermal decomposition product of **3** appears to consist of some mixture of BiOCl (calc. 52.5%) and $Bi_{24}O_{31}Cl_{10}$ (calc 55.5%) (Fig. S21). As the total weight loss for **3** was greater than what could be accounted for as decomposition to either BiOCl or $Bi_{24}O_{31}Cl_{10}$, the onset of $BiCl_3$ sublimation above 300 °C formed *in situ* may account for this discrepancy.[16]

Raman spectroscopy

Raman spectra were collected for **1** and **3** on solid samples of the bulk phases at room temperature (Figs. S22-S23). At lower wavenumbers, the peak around 245 cm^{-1} in each spectrum can be attributed to a ν(Bi-Cl) vibration. Peaks for **1** and **3** in the range of ca. 1000 to 1570 cm^{-1} may be attributed to absorptions from the phen/PDC and terpy ligands, respectively.[64, 71]

Conclusions

Three luminescent bismuth(III)-organic compounds bearing N-donor ligands were synthesized and structurally characterized. The spectroscopic properties of the compounds were also examined. The compounds varied in nuclearity, ranging from monomeric units capped by phenanthroline (**2**) to a dimeric species capped by terpyridine (**3**) to a novel pseudo-tetrameric complex bearing both 2,6-PDC and phenanthroline (**1**). The compounds exhibited visible emission ranging from orange to yellow-green upon UV exposure. Computational analyses aimed at elucidating the emissive pathways were performed and based on these studies the observed luminescence behavior are primarily attributed to ligand-to-ligand and ligand-to-metal charge transfer transitions.

Conflicts of interest

There are no conflicts to declare.

ASSOCIATED CONTENT

Supporting Information.

The Supporting Information is available free of charge on the journal website at DOI: ####.

Crystallographic refinement details; Thermal ellipsoid plots; Powder X-ray Diffractions Patterns; Luminescence Measurements; Raman and UV-vis absorption spectra; TGA plots; and further details of the Computational Analysis.

Accession Codes

CCDC 1841302-1841304 contain the supplementary crystallographic data for this paper. These data can be obtained free of charge via www.ccdc.cam.ac.uk/data_request/cif, or by emailing data_request@ccdc.cam.ac.uk, or by contacting The Cambridge Crystallographic Data Centre, 12 Union Road, Cambridge CD2 1EZ, UK; fax: +44 1223 336033.

AUTHOR INFORMATION

Corresponding Author

*kek44@georgetown.edu

Author Contributions

The manuscript was written through contributions of all authors. All authors have given approval to the final version of the manuscript. † These authors contributed equally to the preparation of this manuscript.

ACKNOWLEDGMENT

The authors gratefully acknowledge the Clare Booth Luce Foundation for their support. The authors would also like to thank the National Science Foundation for acquisition of the single crystal X-ray diffractometer (NSF CHE-1337975) and the Raman spectrometer (NSF CHE-1429079). RLA acknowledges the DoD-SMART Scholarship Program for funding. FR and VV acknowledge support by the French government through the Program "Investissement d'avenir" (LABEX CaPPA / ANR-11-LABX-0005-01 and I-SITE ULNE / ANR-16-IDEX-0004 ULNE), as well as by the Ministry of Higher Education and Research, Hauts de France Council and European Regional Development Fund (ERDF) through the Contrat de Projets État-Région (CPER -CLIMIBIO). Furthermore, this work was granted access to the HPC resources of [CINES/IDRIS/TGCC] under the allocation 2019-2020 [A0050801859] made by GENCI.

ORCID

Alyssa K. Adcock: 0000-0001-9977-3756

R. Lee Ayscue III: 0000-0001-6141-5486

Jeffery A. Bertke: 0000-0002-3419-5163

Florent Réal: 0000-0002-5163-1545

Valérie Vallet: 0000-0002-2202-3858

Karah E. Knope: 0000-0002-5690-715X

REFERENCES

1. Mehring, M., From molecules to bismuth oxide-based materials: Potential homo- and heterometallic precursors and model compounds. *Coordination Chemistry Reviews* **2007,** *251* (7-8), 974-1006.
2. Briand, G. G.; Burford, N., Bismuth compounds and preparations with biological or medicinal relevance. *Chemical Reviews* **1999,** *99* (9), 2601-2657.
3. Yang, N.; Sun, H., Biocoordination chemistry of bismuth: Recent advances. *Coordination Chemistry Reviews* **2007,** *251* (17-20), 2354-2366.
4. Roggan, S.; Limberg, C.; Brandt, M.; Ziemer, B., Organometallic Mo–O–Bi complexes. *Journal of Organometallic Chemistry* **2005,** *690* (23), 5282-5289.
5. Stavila, V.; Davidovich, R. L.; Gulea, A.; Whitmire, K. H., Bismuth(III) complexes with aminopolycarboxylate and polyaminopolycarboxylate ligands: Chemistry and structure. *Coordination Chemistry Reviews* **2006,** *250* (21-22), 2782-2810.

6. Liao, C.; Ma, Z.; Dong, G.; Qiu, J., BiOI nanosheets decorated TiO2 nanofiber: Tailoring water purification performance of photocatalyst in structural and photo-responsivity aspects. *Applied Surface Science* **2014,** *314*, 481-489.

7. Zhang, L.; Yang, J.; Zhao, X. Y.; Xiao, X.; Sun, F. Q.; Zuo, X. X.; Nan, J. M., Small-molecule surface-modified bismuth-based semiconductors as a new class of visible-light-driven photocatalytic materials: Structure-dependent photocatalytic properties and photosensitization mechanism. *Chemical Engineering Journal* **2020,** *380*, 12.

8. U.S. Geological Survey, Bismuth. U.S. Department of the Interior, Ed. 2019; pp 34-35.

9. Sadler, P. J.; Li, H.; Sun, H., Coordination chemistry of metals in medicine: target sites for bismuth. *Coordination Chemistry Reviews* **1999,** *185–186* (0), 689-709.

10. Keogan, D.; Griffith, D., Current and Potential Applications of Bismuth-Based Drugs. *Molecules* **2014,** *19* (9), 15258.

11. Meng, X.; Zhang, Z., Bismuth-based photocatalytic semiconductors: Introduction, challenges and possible approaches. *Journal of Molecular Catalysis A: Chemical* **2016,** *423*, 533-549.

12. Shen, N.; Li, J.; Wu, Z.; Hu, B.; Cheng, C.; Wang, Z.; Gong, L.; Huang, X., α- and β-[Bmim][BiCl4(2,2′-bpy)]: Two Polymorphic Bismuth-Containing Ionic Liquids with Crystallization-Induced Phosphorescence. *Chemistry – A European Journal* **2017,** *23* (62), 15795-15804.

13. Wibowo, A. C.; Vaughn, S. A.; Smith, M. D.; zur Loye, H.-C., Novel Bismuth and Lead Coordination Polymers Synthesized with Pyridine-2,5-Dicarboxylates: Two Single Component “White” Light Emitting Phosphors. *Inorganic Chemistry* **2010,** *49* (23), 11001-11008.

14. Wibowo, A. C.; Smith, M. D.; zur Loye, H.-C., Structural Diversity of Metal-Organic Materials Containing Bismuth(III) and Pyridine-2,5-Dicarboxylate. *Crystal Growth & Design* **2011,** *11* (10), 4449-4457.

15. Wibowo, A. C.; Smith, M. D.; zur Loye, H. C., A new Kagome lattice coordination polymer based on bismuth and pyridine-2,5-dicarboxylate: structure

and photoluminescent properties. *Chemical Communications* **2011,** *47* (26), 7371-7373.

16. Heine, J.; Wehner, T.; Bertermann, R.; Steffen, A.; Muller-Buschbaum, K., $_{(2)(\text{infinity})}$ $Bi_2Cl_6(pyz)_{(4)}$: A 2D-Pyrazine Coordination Polymer As Soft Host Lattice for the Luminescence of the Lanthanide Ions Sm^{3+}, Eu^{3+}, Tb^{3+}, and Dy^{3+}. *Inorganic Chemistry* **2014,** *53* (14), 7197-7203.

17. Sorg, J. R.; Wehner, T.; Matthes, P.; Sure, R.; Grimme, S.; Heine, J.; Muller-Buschbaum, K., Bismuth as Versatile Cation for Luminescence in Coordination Polymers from BiX3/4,4'-bipy: Understanding of Photophysics by Quantum Chemical Calculations and Structural Parallels to Lanthanides. *Dalton Transactions* **2018**.

18. Zhang, X. P.; Tian, H. R.; Yan, G. F.; Su, Y.; Feng, Y. L.; Cheng, J. W., Incorporating different secondary building units of {Bi-2}, {Bi-8} and {Bi-10} to construct diversity of luminescent bismuth-organic frameworks. *Dalton Transactions* **2013,** *42* (4), 1088-1093.

19. Thirumurugan, A.; Cheetham, A. K., Anionic Metal–Organic Frameworks of Bismuth Benzenedicarboxylates: Synthesis, Structure and Ligand-Sensitized Photoluminescence. *European Journal of Inorganic Chemistry* **2010,** *2010* (24), 3823-3828.

20. Yu, X.; Zhang, H.; Cao, Y.; Hu, Z.; Chen, Y.; Wang, Z., Two novel 3-D bismuth oxalates with organic amines protruding in channels. *Journal of Solid State Chemistry* **2006,** *179* (10), 3095-3100.

21. Feyand, M.; Köppen, M.; Friedrichs, G.; Stock, N., Bismuth Tri- and Tetraarylcarboxylates: Crystal Structures, In Situ X-ray Diffraction, Intermediates and Luminescence. *Chemistry – A European Journal* **2013,** *19* (37), 12537-12546.

22. Sorg, J. R.; Schneider, T.; Wohlfarth, L.; Schäfer, T. C.; Sedykh, A.; Müller-Buschbaum, K., Sb- and Bi-based coordination polymers with N-donor ligands with and without lone-pair effects and their photoluminescence properties. *Dalton Transactions* **2020,** *49* (15), 4904-4913.

23. Adcock, A. K.; Gibbons, B.; Einkauf, J. D.; Bertke, J. A.; Rubinson, J. F.; de Lill, D. T.; Knope, K. E., Bismuth(III)-thiophenedicarboxylates as host frameworks

for lanthanide ions: synthesis, structural characterization, and photoluminescent behavior. *Dalton Transactions* **2018,** *47* (38), 13419-13433.

24. Vogler, A.; Nikol, H., Photochemistry and photophysics of coordination compounds of the main group metals. *Pure and Applied Chemistry* **1992,** *64* (9), 1311.

25. Adcock, A. K.; Batrice, R. J.; Bertke, J. A.; Knope, K. E., Structural Diversity of Bismuth(III) Thiophenemonocarboxylates Isolated from Aqueous Solutions. *European Journal of Inorganic Chemistry* **2017,** (11), 1435-1445.

26. Luckay, R.; Cukrowski, I.; Mashishi, J.; H. Reibenspies, J.; H. Bond, A.; D. Rogers, R.; D. Hancock, R., Synthesis, stability and structure of the complex of bismuth(III) with the nitrogen-donor macrocycle 1,4,7,10-tetraazacyclododecane. The role of the lone pair on bismuth(III) and lead(II) in determining co-ordination geometry. *Journal of the Chemical Society, Dalton Transactions* **1997,** (5), 901-908.

27. Briand, G. G.; Burford, N., Coordination complexes of bismuth(III) involving organic ligands with pnictogen or chalcogen donors. In *Advances in Inorganic Chemistry*, Academic Press: 2000; Vol. 50, pp 285-357.

28. Toma, O.; Mercier, N.; Botta, C., N-Methyl-4,4′-bipyridinium and N-Methyl-N′-oxide-4,4′-bipyridinium Bismuth Complexes – Photochromism and Photoluminescence in the Solid State. *European Journal of Inorganic Chemistry* **2013,** *2013* (7), 1113-1117.

29. Cunha, C. S.; Köppen, M.; Terraschke, H.; Friedrichs, G.; Malta, O. L.; Stock, N.; Brito, H. F., Luminescence tuning and single-phase white light emitters based on rare earth ions doped into a bismuth coordination network. *Journal of Materials Chemistry C* **2018,** *6* (46), 12668-12678.

30. Thirumurugan, A.; Li, W.; Cheetham, A. K., Bismuth 2,6-pyridinedicarboxylates: Assembly of molecular units into coordination polymers, CO2 sorption and photoluminescence. *Dalton Transactions* **2012,** *41* (14), 4126-4134.

31. Adonin, S. A.; Sokolov, M. N.; Rakhmanova, M. E.; Smolentsev, A. I.; Korolkov, I. V.; Kozlova, S. G.; Fedin, V. P., Luminescent properties of 4,4-

bipyridinium chlorobismuthate salt: Strong influence of solvation. *Inorganic Chemistry Communications* **2015,** *54*, 89-91.

32. Accorsi, G.; Listorti, A.; Yoosaf, K.; Armaroli, N., 1,10-Phenanthrolines: versatile building blocks for luminescent molecules, materials and metal complexes. *Chemical Society Reviews* **2009,** *38* (6), 1690-1700.

33. Mürner, H.-R.; Chassat, E.; Thummel, R. P.; Bünzli, J.-C. G., Strong enhancement of the lanthanide-centred luminescence in complexes with 4-alkylated 2,2′;6′,2″-terpyridines. *Journal of the Chemical Society, Dalton Transactions* **2000,** (16), 2809-2816.

34. Zhang, X.-P.; Wang, D.-G.; Su, Y.; Tian, H.-R.; Lin, J.-J.; Feng, Y.-L.; Cheng, J.-W., Luminescent 2D bismuth–cadmium–organic frameworks with tunable and white light emission by doping different lanthanide ions. *Dalton Transactions* **2013,** *42* (29), 10384-10387.

35. Qi, H.-X.; Jo, H.; Chen, X.; Hong, J.; Ok, K. M., Second-Harmonic Generation and Photoluminescence Properties of Sn(II)- and Bi(III)-Based Lone Pair Cation–Pyridine Dicarboxylate Coordination Compounds. *Inorganic Chemistry* **2020**.

36. Ayscue, R. L.; Verwiel, C. P.; Bertke, J. A.; Knope, K. E., Excitation-Dependent Photoluminescence Color Tuning in Lanthanide-Organic Hybrid Materials. *Inorganic Chemistry* **2020,** *59* (11), 7539-7552.

37. Batrice, R. J.; Ayscue, R. L., III; Adcock, A. K.; Sullivan, B. R.; Han, S. Y.; Piccoli, P. M.; Bertke, J. A.; Knope, K. E., Photoluminescence of Visible and NIR-Emitting Lanthanide-Doped Bismuth-Organic Materials. *Chemistry - A European Journal* **2018,** *24* (21), 5630-5636.

38. Batrice, R. J.; Ridenour, J. A.; Ayscue, R. L., III; Bertke, J. A.; Knope, K. E., Synthesis, structure, and photoluminescent behaviour of molecular lanthanide-2-thiophenecarboxylate-2,2′:6′,2″-terpyridine materials. *CrystEngComm* **2017,** *19* (35), 5300-5312.

39. Carter, K. P.; Zulato, C. H. F.; Cahill, C. L., Exploring supramolecular assembly and luminescent behavior in a series of RE-p-chlorobenzoic acid-1,10-phenanthroline complexes. *CrystEngComm* **2014,** *16* (44), 10189-10202.

40. Carter, K. P.; Thomas, K. E.; Pope, S. J. A.; Holmberg, R. J.; Butcher, R. J.; Murugesu, M.; Cahill, C. L., Supramolecular Assembly of Molecular Rare-Earth-3,5-Dichlorobenzoic Acid-2,2':6',2''-Terpyridine Materials: Structural Systematics, Luminescence Properties, and Magnetic Behavior. *Inorganic Chemistry* **2016,** *55* (14), 6902-6915.

41. Janiak, C., A critical account on π–π stacking in metal complexes with aromatic nitrogen-containing ligands. *Journal of the Chemical Society, Dalton Transactions* **2000,** (21), 3885-3896.

42. Bowmaker, G. A.; Hannaway, F. M. M.; Junk, P. C.; Lee, A. M.; Skelton, B. W.; White, A. H., Synthetic, Structural and Vibrational Spectroscopic Studies in Bismuth(III) Halide/N,N′-Aromatic Bidentate Base Systems. V Bismuth(III) Halide/N,N′-Bidentate Ligand (1 : 2) Systems. *Australian Journal of Chemistry* **1998,** *51* (4), 325-330.

43. *SAINT*, Bruker AXS Inc.: Madison, WI, USA, 2007.

44. Fox, A. R.; Bart, S. C.; Meyer, K.; Cummins, C. C., Towards uranium catalysts. *Nature* **2008,** *455* (7211), 341-349.

45. Sheldrick, G., A short history of SHELX. *Acta Crystallographica Section A* **2008,** *64* (1), 112-122.

46. Farraguia, L. J., *Journal of Applied Crystallography* **2012,** *45*, 849-845.

47. Spek, A., Structure validation in chemical crystallography. *Acta Crystallographica Section D* **2009,** *65* (2), 148-155.

48. Neese, F., The ORCA program system. *Wiley Interdiscip. Rev.: Computational Molecular Science* **2012,** *2*, 73-78.

49. Neese, F. 4.3; 2019.

50. Yanai, T.; Tew, D. P.; Handy, N. C., *Chemical Physical Letters* **2004,** *393*, 51-57.

51. Weigend, F.; Ahlrichs, R., Balanced basis sets of split valence, triple zeta valence and quadruple zeta valence quality for H to Rn: Design and assessment of accuracy. *Physical Chemistry Chemical Physics* **2005,** *7* (18), 3297-3305.

52. Metz, B.; Stoll, H.; Dolg, M., Small-core multiconfiguration-Dirac–Hartree–Fock-adjusted pseudopotentials for post-d main group elements: Application to PbH and PbO. *The Journal of Chemical Physics* **2000,** *113* (7), 2563-2569.

53. Neese, F.; Wennmohs, F.; Hansen, A.; Becker, U., Efficient, approximate and parallel Hartree–Fock and hybrid DFT calculations. A 'chain-of-spheres' algorithm for the Hartree–Fock exchange. *Chemical Physics* **2009,** *356* (1), 98-109.

54. Petrenko, T.; Kossmann, S.; Neese, F., Efficient time-dependent density functional theory approximations for hybrid density functionals: Analytical gradients and parallelization. *The Journal of Chemical Physics* **2011,** *134* (5), 054116.

55. Bannwarth, C.; Grimme, S., *Computational and Theoretical Chemistry* **2014,** *1040*, 45-53.

56. Grimme, S., A simplified Tamm-Dancoff density functional approach for the electronic excitation spectra of very large molecules. *The Journal of Chemical Physics* **2013,** *138* (24), 244104.

57. Risthaus, T.; Hansen, A.; Grimme, S., Excited states using the simplified Tamm–Dancoff-Approach for range-separated hybrid density functionals: development and application. *Physical Chemistry Chemical Physics* **2014,** *16* (28), 14408-14419.

58. te Velde, G.; Bickelhaupt, F. M.; Baerends, E. J.; Fonseca Guerra, C.; van Gisbergen, S. J. A.; Snijders, J. G.; Ziegler, T., Chemistry with ADF. *Journal of Computational Chemistry* **2001,** *22* (9), 931-967.

59. Fonseca Guerra, C.; Snijders, J. G.; te Velde, G.; Baerends, E. J., Towards an order-N DFT method. *Theoretical Chemistry Accounts* **1998,** *99* (6), 391-403.

60. Baerends, E. J.; Ziegler, T.; A.J. Atkins; J. Autschbach; O. Baseggio; D. Bashford; A. Bérces; F.M. Bickelhaupt; C. Bo; P.M. Boerrigter; L. Cavallo; C. Daul; D.P. Chong; D.V. Chulhai; L. Deng; R.M. Dickson; J.M. Dieterich; D.E. Ellis; M. van Faassen; L. Fan, T. H. F.; C. Fonseca Guerra; M. Franchini; A. Ghysels; A. Giammona; S.J.A. van Gisbergen; A. Goez; A.W. Götz; J.A. Groeneveld; O.V. Gritsenko; M. Grüning; S. Gusarov; F.E. Harris; P. van den Hoek; Z. Hu; C.R. Jacob; H. Jacobsen; L. Jensen; L. Joubert; J.W. Kaminski; G. van Kessel; C. König; F. Kootstra; A. Kovalenko; M.V. Krykunov; E. van Lenthe; D.A. McCormack;

A. Michalak; M. Mitoraj; S.M. Morton; J. Neugebauer; V.P. Nicu; L. Noodleman; V.P. Osinga; S. Patchkovskii; M. Pavanello; C.A. Peeples; P.H.T. Philipsen; D. Post; C.C. Pye; H. Ramanantoanina; P. Ramos; W. Ravenek; J.I. Rodríguez; P. Ros; R. Rüger; P.R.T. Schipper; D. Schlüns; H. van Schoot; G. Schreckenbach; J.S. Seldenthuis; M. Seth; J.G. Snijders; M. Solà; M. Stener; M. Swart; D. Swerhone; V. Tognetti; G. te Velde; P. Vernooijs; L. Versluis; L. Visscher; O. Visser; F. Wang; T.A. Wesolowski; E.M. van Wezenbeek; G. Wiesenekker; S.K. Wolff, T.; .K. Woo; Yakovlev, A. L. Vrije Universiteit, Amsterdam, The Netherlands, http://www.scm.com. , 2019.

61. Mitoraj, M. P.; Michalak, A.; Ziegler, T., A Combined Charge and Energy Decomposition Scheme for Bond Analysis. *Journal of Chemical Theory and Computation* **2009,** *5* (4), 962-975.

62. Mitoraj, M. P.; Michalak, A.; Ziegler, T., On the Nature of the Agostic Bond between Metal Centers and β-Hydrogen Atoms in Alkyl Complexes. An Analysis Based on the Extended Transition State Method and the Natural Orbitals for Chemical Valence Scheme (ETS-NOCV). *Organometallics* **2009,** *28* (13), 3727-3733.

63. Frank, W.; Reiland, V., Heavy-Metal [pi] Complexes. 13. Trichloro(1,2,3-trimethylbenzene)bismuth(III). *Acta Crystallographica Section C* **1998,** *54* (11), 1626-1628.

64. Zhang, W.; Feng, Y.-Q., A novel dinuclear bismuth(III) coordination compound: bis([mu]-pyridine-2,6-dicarboxylato)-[kappa]4O2,N,O6:O6';[kappa]4O2:O2',N,O6-bis[(azido-[kappa]N)(1,10-phenanthroline-[kappa]2N,N')bismuth(III)] tetrahydrate. *Acta Crystallographica Section C* **2014,** *70* (6), 562-565.

65. Lewis, K. M.; Kelley, J.; Peterson, L.; Smith, M. D.; Severance, R. C.; Vaughn, S. A.; Loye, H.-C. z., Synthesis and Crystal Structure of an Iodobismuthate Incorporating Both a Cationic and Anionic Bi (III) Complex Ion. *Journal of Chemical Crystallography* **2010,** *40* (10), 867-871.

66. Raston, C. L.; Rowbottom, G. L.; White, A. H., Structural studies of Group 5B-halide-dithio-ligand complexes. Part 7. Crystal structures of the 1 : 1 adducts of

(NN-diethyldithiocarbamato)-di-iodobismuth(III) with 2,2'-bipyridyl and 2,2':6',2'-terpyridyl. *Dalton Transactions* **1981,** (6), 1383-1388.

67. Tershansy, M. A.; Goforth, A. M.; Smith, M. D.; zur Loye, H.-C., The Synthesis and Crystal Structure of [BiI2(tpy)2][Bi2I7(tpy)]: A New Metal Halide Material. *Journal of Chemical Crystallography* **2008,** *38* (6), 453-459.

68. Junk, P. C.; Louis, L. M., Dimeric Structure of [(η2-NO3)2(tpy)Bi(μ-OH)2Bi(tpy)(η2-NO3)2]. *Zeitschrift für anorganische und allgemeine Chemie* **2000,** *626* (2), 556-559.

69. Evans, W. J.; Hain, J. H.; Ziller, J. W., Synthesis and first X-ray crystal structure of a $Bi(OR)_3$ complex: tris(2,6-dimethylphenoxo)bismuth. *Journal of the Chemical Society, Chemical Communications* **1989,** (21), 1628-1629.

70. Ouerghi, Z.; Gornitzka, H.; Temel, E.; Dridi, I.; Kefi, R., A new non-centrosymmetric Chlorobismuthate(III) hybrid material: Crystal structure, optical properties and antibacterial study. *Journal of Molecular Structure* **2019,** *1181*, 338-347.

71. Yin, H. D.; Wang, C. H.; Xing, Q. J., Synthesis and Crystal Structure of Bismuth(III) Complexes $Bi(1,10\text{-phen})[S_2CN(CH_3)_2]_2(NO_3)$, $\{Bi(S_2COCH_2)[S_2CNC_6H_5(CH_3)]_2\}_2$ and $[Bi(S_2CNBu_2)_2(CH_3OH)(NO_3)]_\infty$. *Chinese Journal of Chemistry* **2005,** *23* (12), 1631-1636.

TOC entry

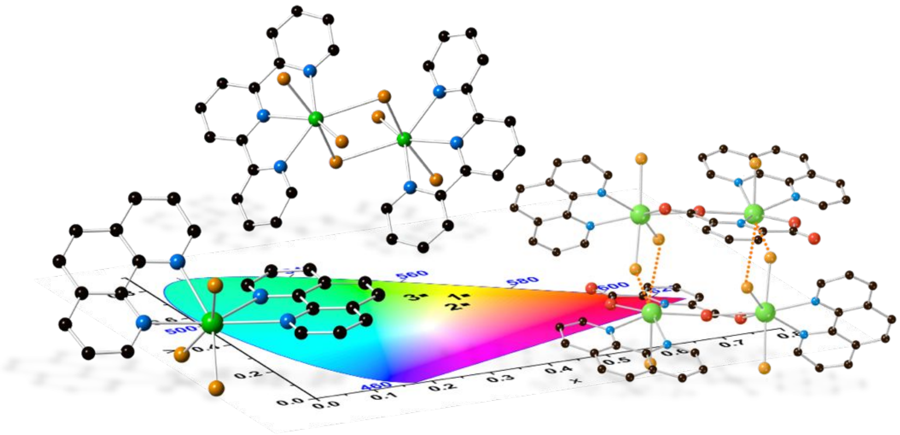

The synthesis and structural characterization of three bismuth-based materials that exhibit visible emission attributed to ligand-to-ligand and/or LMCT are reported.